frontiers | Frontiers in Earth Science

TYPE Original Research
PUBLISHED 12 October 2022
DOI 10.3389/feart.2022.1030417

OPEN ACCESS

EDITED BY
Zizheng Guo,
Hebei University of Technology, China
orcid.org/0000-0003-0404-3430

REVIEWED BY
Xiaoge Liu,
Central South University, China
Ahmad Rashidi,
International Institute of Earthquake Engineering and Seismology, Iran
Layue Li,
China Earthquake Administration, China
Dimas Sianipar,
Climatology and Geophysics, Indonesia

*CORRESPONDENCE
Chong Xu,
xc11111111@126.com

SPECIALTY SECTION
This article was submitted to Geohazards and Georisks, a section of the journal Frontiers in Earth Science

RECEIVED 28 August 2022
ACCEPTED 20 September 2022
PUBLISHED 12 October 2022

CITATION
He X and Xu C (2022), Spatial distribution and tectonic significance of the landslides triggered by the 2021 Ms6.4 Yangbi earthquake, Yunnan, China.
Front. Earth Sci. 10:1030417.
doi: 10.3389/feart.2022.1030417

Spatial distribution and tectonic significance of the landslides triggered by the 2021 Ms6.4 Yangbi earthquake, Yunnan, China

Xiangli He[1,2,3] and Chong Xu[1,2,3]*

[1]National Institute of Natural Hazards, Ministry of Emergency Management of China, Beijing, China, [2]Key Laboratory of Compound and Chained Natural Hazards Dynamics (Under Construction), Ministry of Emergency Management of China, Beijing, China, [3]Key Laboratory of Landslide Risk Early-Warning and Control, Ministry of Emergency Management of China, Chengdu, China

An Ms6.4 earthquake occurred on 21 May 2021 in Yangbi County, Yunnan Province, located in the strong earthquake hazard zone, the border of the Sichuan-Yunnan rhomb block, southeast Tibetan Plateau, causing severe loss of life and property. Adequate research on the distribution characteristics and seismotectonic mechanisms of seismic chain-generated hazards in the region is meaningful for mitigating seismic hazard risks. In this paper, based on the interpretation of remote sensing satellite images and the analysis on GeoScene platform, we compile a detailed inventory of landslides induced by the Yangbi earthquake and analyze the correlation of their spatial distribution with the influence factors. The results show that 95 landslides were interpreted, and their spatial distribution is correlated to the topographic, seismic and geological factors. Statistically, the landslide number and mobility increase with the slope angle; the south- and southeast-facing slopes and weaker metamorphic rocks are more prone to landslides; the higher the seismic intensity, the larger the density and scale of landslides. Furthermore, the development of the landslides is not only influenced by the Ms6.4 mainshock, but also by the Ms5.6 foreshock, which is significantly correlated with the size of landslides. Notably, the long axis of the landslide distribution area is in NW-SE direction, which is nearly parallel to the strike of the Weixi-Qiaohou-Weishan fault zone (WQWF). The landslides are mainly distributed in the southwest wall and southeast section of the fault. The landslide number and density unstably decrease with the vertical distance from the fault with many fluctuations. Combined with the previous studies, two possible seismogenic structure models are inferred. One model is a parallel secondary fault of the WQWF, Another one is a flower structure in the southwest wall of the WQWF. Both models are mainly characterized by right-lateral strike slip with a small normal-fault component. Additionally, the seismic rupture propagated mainly to the southeast along the seismogenic fault in the subsurface without surface rupture.

KEYWORDS

Yangbi earthquake, landslide inventory, spatial distribution, influence factors, seismogenic fault

1 Introduction

On 21 May 2021, at 21:48 (Beijing time), an Ms6.4 earthquake occurred in Yangbi County, Yunnan Province, China (hereafter called "Yangbi earthquake"), with the epicenter at 99.87°E, 25.67°N, and the source depth of 8 km (CENC, http://www.cenc.ac.cn). This earthquake is another devastating earthquake that occurred at the border of the Sichuan-Yunnan rhomb block following the 2014 Ludian Ms6.5 and Jinggu Ms6.6 earthquakes (Figure 1B), causing more than 30 deaths and injuries, 92 house collapses, 13,090 house damages, and damage to other infrastructures (Yang et al., 2021). The region is the southeastern bend of the Tethys-Himalayan tectonic system, where the crust undergoes clockwise rotational motion, and there is a channel of material extrusion from the Qinghai-Tibet Plateau to the southeast (Gan et al., 2022). The complex tectonic environment there attractsexcellent concerns for strong earthquakes. Therefore, it is necessary to conduct sufficient research on the earthquake mechanism and the distribution characteristics of earthquake chain-generated geological hazards in the region to provide guidance and a basis for earthquake hazard risk mitigation.

Recently, many scholars have studied the deep tectonic background and seismogenic mechanism of the Yangbi earthquake through field investigation, geomagnetic, and seismic sequence, *etc.* (Li et al., 2021, 2022; Yang et al., 2021; Liu et al., 2021; Long et al., 2021; Ye et al., 2021; Liu X et al., 2022; Liu et al., 2022). Since no apparent surface rupture phenomenon was found during the earthquake fieldwork (Li et al., 2021), there are some difficulties in understanding the seismogenic structure. Based on the above methods, most studies tentatively concluded that the seismogenic structure was a parallel associated fault or a

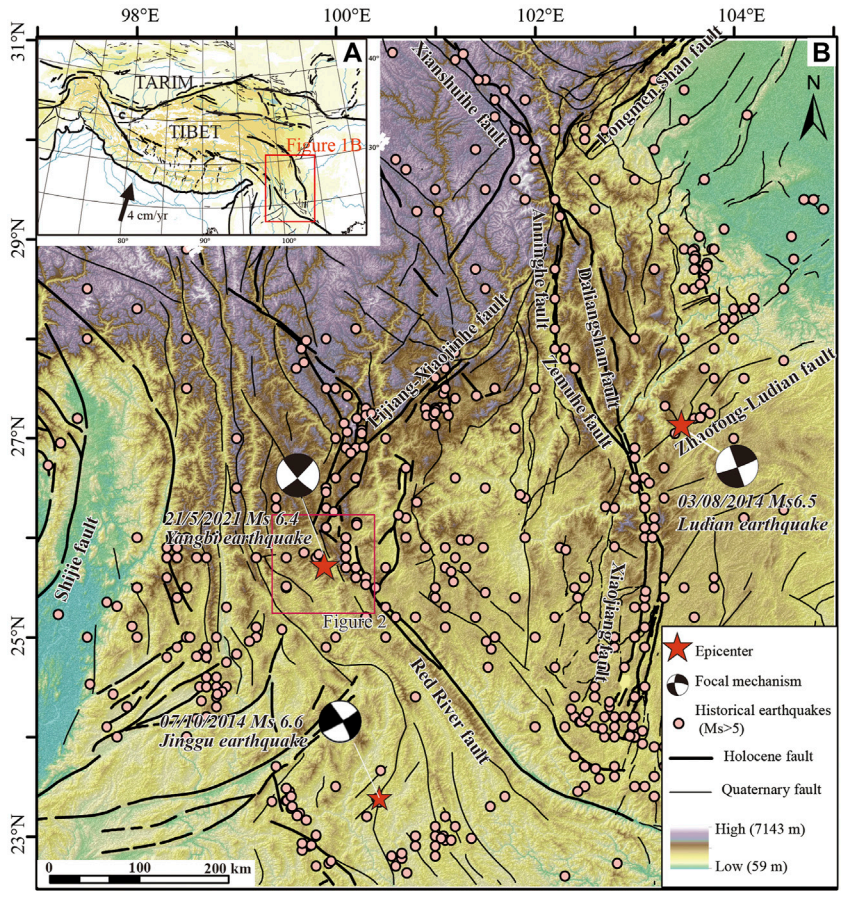

FIGURE 1
Maps showing the tectonic setting of the 2021 Yangbi earthquake. **(A)** The simplified tectonic map of Tibetan plateau and adjacent regions. **(B)** The tectonic setting and historical earthquakes (Ms>5) of Sichuan-Yunnan rhomb block in the southeastern margin of Tibetan Plateau.

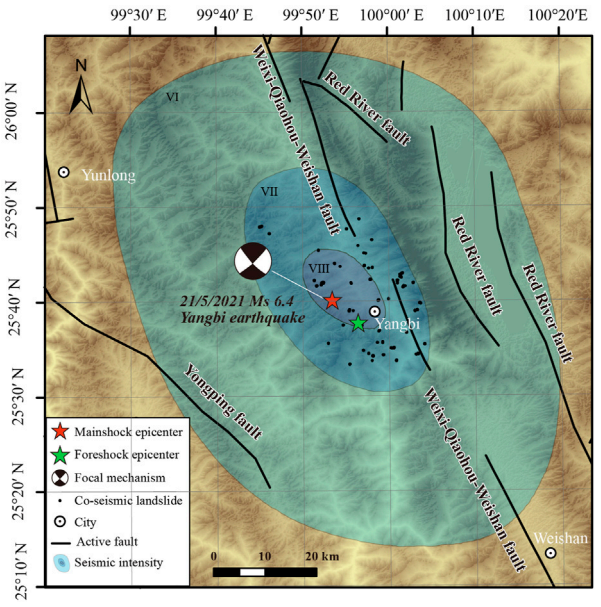

FIGURE 2
Map showing the distribution of faults, seismic intensity, and co-seismic landslides in the 2021 Yangbi earthquake area.

hidden branch of the Weixi-Qiaohou-Weishan fault (WQWF, Figure 2; Liu et al., 2021; Yang et al., 2021). However, it is still controversial to determine the seismogenic structure (Li et al., 2021; Lei et al., 2021; Su et al., 2021; Wang et al., 2021). For example, Wang et al. (2021) suggested the Caoping fault that was reversed and left-lateral strike-slip at an early stage, and Li et al. (2021) proposed the newer Yanke-Shahe fault. It needs to be verified with more evidence.

Co-seismic landslides are a kind of surface change during earthquakes, which are caused by strong shaking or obvious surface deformation generated by earthquakes. Therefore, the spatial distribution of co-seismic landslides often shows a close correlation with the earthquake epicenter and seismogenic structures that release seismic energy (Keefer 2000; Mahdavifar et al., 2006; Meunier et al., 2013; Xu et al., 2014; Gorum et al., 2014; Valagussa et al., 2019). For instance, there is a negative relation between the distance to the epicenter and the landslide number (Papadopoulos and Plessa 2000). Landslides often symmetrically distribute on both sides of a strike-slip seismogenic fault (Gorum et al., 2014), and mainly occur on the hanging wall of an oblique-slip seismogenic fault (Tatard and Grasso, 2013; Xu et al., 2014), and are more scattered in the vicinity of a blind seismogenic fault (Xu, 2014). Accordingly, the data on the spatial distribution pattern of co-seismic landslides, including the number, density, and scale of landslides, is essential for understanding the seismogenic mechanisms. Co-seismic landslides are also a fundamental cause of human casualties and building damage in earthquakes. Their formation and distribution are influenced by multiple factors such as topography (elevation, aspect, slope angle, curvature), seismic parameters, slope materials (soil cover and lithology), hydrology, geomorphology, and land use (Gorum et al., 2011; Xu C. et al., 2014; Tanyaş et al., 2017; Roback et al., 2018; Tanyaş et al., 2019; Shao and Xu 2022). Mapping of landslides and their statistical studies (Huang et al., 2020a; Chang et al., 2020; Huang et al., 2022) and landslide susceptibility models that consider different influence factors are also useful for our understanding of landslide hazard risk (Jiang et al., 2018; Huang et al., 2020b; Huang et al., 2020c; Chang et al., 2022). A detailed understanding of the multi-factor interplayed causal mechanisms of co-seismic landslides in this high-risk seismic region of western Yunnan is essential for the future mitigation of the seismic chain-generated hazards. However, there are few studies on the Yangbi earthquake-triggered landslides. Zhou et al. (2022) only studied the characteristics and failure mechanisms of landslides along the highway in the Yangbi earthquake, without the landslide distribution characteristics in the whole seismic area.

In this paper, a Yangbi earthquake-triggered landslide inventory is compiled based on an online interpretation of satellite images. The spatial distribution characteristics of these landslides in the classifications of multiple factors, including topography factors (relief, slope, aspect, curvature), geology factors (strata, faults), and earthquakes factors (epicenter, intensity, co-seismic deformation), are described by parameters such as landslide number, landslide number density, and average area of landslides. Finally, we analyze the correlation between these factors and landslide distribution and discuss the tectonic mechanism of the Yangbi earthquake according to the distribution pattern of co-seismic landslides and the results of previous studies.

2 Tectonic setting

The Ms6.4 earthquake occurred in Yangbi County, Dali Prefecture, Yunnan Province on 21 May 2021 (99.87°E, 25.67°N). Tectonically, the earthquake is located at the southeastern margin of the Tibetan Plateau, the western boundary of the Sichuan-Yunnan rhombic block, and near the west side of the Red River fault (Figure 1), which is a discrete zone extruding from the Tibetan Plateau to the southeast (Yang et al., 2021; Long et al., 2021). The Sichuan-Yunnan rhombic block is blocked by the South China block and escapes to the SSE (Figure 1), which is the most active block with vigorous seismotectonic activity (Wang et al., 200L; Zhang et al., 2004; Shen et al., 2005; Deng et al., 2014).

The large-scale fault zones in the adjacent area of the earthquake are intertwined, including the Nujiang fault and Lancangjiang fault in the near SN direction, the Jinshajiang

fault and the Red River fault in the NW direction, the Xiaojinhe-Lijiang fault and the Nantinghe fault in the NE direction, etc. (Figure 1B; Xu et al., 2014; Li et al., 2021). Among them, the Red River fault is a large right-lateral strike-slip shear zone at the southwest boundary of the Sichuan-Yunnan block, which plays a vital role in the evolution of the crust and intracontinental tectonic deformation in the region (Tapponnier et al., 1990, 2001; Leloup et al., 1995). Its slip rate is about 5 mm/a in the late Quaternary, and several strong earthquakes of magnitude ~7 have occurred along this fault (Tapponnier et al., 1990; Leloup et al., 1995; Tapponnier et al., 2001). The WQWF is located on the west side of the Red River fault, a known fault closest to the Yangbi earthquake (Figures 1, 2). It is connected to the Jinshajiang fault in the north and the Red River fault in the south, and shows prominent right-lateral strike-slip characteristics in the late Quaternary, which is in line with the Red River fault zone in some scholars' opinion due to their same movement characteristics (Ren et al., 2007; Chang et al., 2014, 2016). The WQWF is mainly NNW-SSE trending and dips to the southwest with a steep dip angle. It starts from Baijixun region at the eastern foot of the Xuelong Mountains in the north, going southeastward through Weixi, Tongdian, Qiaohou, and ending at the southern end of the Weishan Basin, with a length of about 280 km (Figure 2). Longitudinally, the WQWF can be divided into the northern, middle, and southern sections with bounds of Yushichang and Pingpo. The north and central sections are mainly right-lateral strike-slip during the Neotectonic period, while the southern section (Weishan Basin section) is primarily a normal-fault movement characteristic. Laterally, it can be divided into two branches: the eastern branch connects with the Red River fault zone through Damaidi, and the western branch extends to the Weishan area (Li et al., 2021).

Although the magnitudes of most historical earthquakes along the WQWF are less than five, some moderate-strong earthquakes occurred in the study area, such as the 1948 M6.25 earthquake at Jianchuanshanglan (Chang et al., 2016), 2013 Ms5.5 Eryuan earthquake (Zhao and Fu, 2014), 2016 Ms5.0 Yunlong earthquake (Jiang et al., 2019), and 2017 Ms5.1 Yangbi earthquake (Pan et al., 2019). Additionally, some scholars have uncovered paleoseismic remains in the vicinity of Tongdian Basin and Yushichang, indicating that the WQWF has been ruptured to the surface several times by strong seismic events since the late Pleistocene (Chang et al., 2018). These earthquakes prove that the WQWF has been active, and the distribution of historical earthquakes shows that the central part of the fault is more active (Figure 1B). The highest seismic intensity of this earthquake is VIII degree, and the area above the VI degree zone is about 6600 km^2, involving 6 counties and cities in Dali Prefecture, with a long axis of NNW-SSE direction (Figure 2; Yunnan Earthquake Bureau, 2021).

3 Data and methods

A detailed and complete co-seismic landslide database is significant for studying their spatial distribution pattern, hazard risk assessment, and seismic mechanism (Keefer, 2002; Khattak et al., 2010; Dai et al., 2011; Harp et al., 2011; Xu et al., 2014; Fan et al., 2019; Xu and Xu, 2021). In this work, we compared the Planet satellite image data (with a resolution of 3 m) before and after the earthquake. The pre-quake images were acquired in April 2021, and post-quake images were acquired in Agust, 2021, which were the most available images to distinguish the coseismic landslides effectively. The images closer to the occurrence time of the Yangbi earthquake were covered by a large area of clouds. We identified co-seismic landslides based on the differences in information such as color, texture, and vegetation cover of the images, as shown in Figure 3, with the development characteristics of landslides in the field (Xu, 2015). Polygons were used to outline the landslide boundary, which can indicate the landslide size (Harp and Jibson, 1995), and the point showing the center of gravity of each polygon was extracted to present the landslide location on GeoScene platform (Figure 3).

This study analyzed the relationship between three influence factors (topographic, seismic, and geological) and the Yangbi earthquake-triggered landslides. Topographic factors include topographic relief, slope angle, slope direction (aspect), and slope curvature. These factors were extracted from the 30-m resolution ASTGTM digital elevation model (DEM) from Geospaial Data Cloud (http://www.gscloud.cn/sources/accessdata/310?pid=302). Topographic relief, the elevation difference between the target point and the lowest point in the study area, was divided into 10 categories with a spacing of 200 m. The slope angle is divided into 7 categories with a spacing of 10°. The aspect is divided into 9 categories: north, northeast, east, southeast, south, southwest, west, northwest and the flat area. Slope curvature is divided into 6 categories according to the degree of concavity and convexity. According to the seismic sequence records, this earthquake is a typical foreshock-mainshock-aftershock type event. The largest foreshock is the Ms5.6 earthquake which occurred 27 min before the mainshock, about 6 km away from the Ms6.4 mainshock epicenter (Liu et al., 2021; Long et al., 2021). The seismic factors include the seismic intensity, the co-seismic deformation, the distance from the Yangbi mainshock's epicenter, the distance from the epicenter of the Ms5.6 foreshock and the combined effect of both earthquakes. The seismic intensity data were provided by Earthquake Administration of Yunnan Province (http://www.yndzj.gov.cn/). The locations of epicenters reported by China Earthquake Networks Center (https://news.ceic.ac.cn/; Yang et al., 2021) were used. The data of the co-seismic deformation were obtain from (Liu et al., 2022).

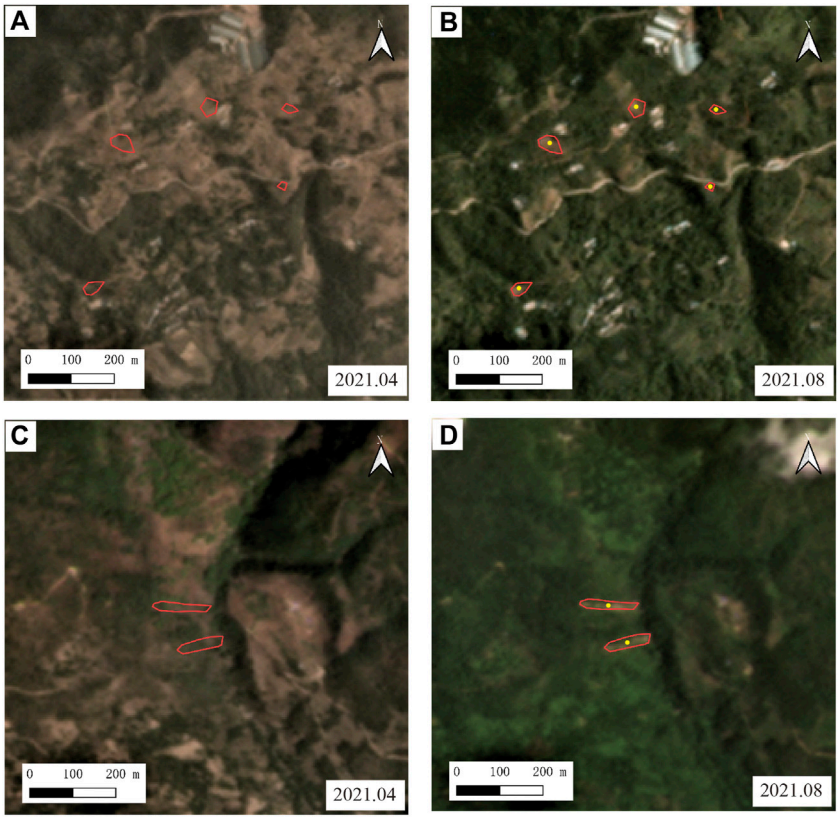

FIGURE 3
Two representative cases of landslides from interpretation by comparing post- and pre-earthquake satellite images. **(A,B)** The regional center is located at 99.871°E, 25.698°N. **(C,D)** The regional center is located at 99.968° E, 25.57°N. Pre-earthquake ones were acquired in April 2021, and post-earthquake ones in August 2020. Red lines and yellow dots respectively show the boundaries and locations of identified landslides.

Stratigraphic lithology and the vertical and parallel distances of the nearest fault (WQWF) are considered as geological factors. The stratigraphic data were obtained in the 1:200,000 geologic map from National Geological Archives of China (http://www.ngac.org.cn/DataSpecial/geomap.html), and the fault locations were taken from the national distribution map of active faults (Deng et al., 2003). The distances from the epicenters and fault are classified at 2 km intervals. The stratigraphy of the study area includes five chronostratigraphic strata, namely the Quaternary, Tertiary, Cretaceous, Jurassic and Triassic.

The maximum intensity of this earthquake is VIII degrees on the Chinese seismic intensity scale, and the co-seismic landslides are distributed in VII- and VIII-degrees zones (Figure 2). In this paper, two intensity zones, VII and VIII, are selected as the study area to carry out the analysis of the spatial distribution pattern of co-seismic landslides. We used the parameters, such as the area of each factor classification (CA), landslide number (LN), landslide number density (LND=LN/CA), and average landslide area (ALA=TLA/LN, TLA is the total landslides area) to analyze the spatial distribution of co-seismic landslides in each factor classifications. In addition, the difference between the highest and lowest elevation of each landslide boundary (H) and the farthest horizontal distance between such two points (L) was obtained in this study. The L is calculated by the longitude (X) and latitude (Y) of two points, as shown in the Eq. 1. Based on the landslide mobility index (H/L), the mobility of the Yangbi earthquake-triggered landslides was analyzed. Finally, we summarized the controlling factors that have a strong influence on the landslide distribution and discussed the seismogenic faults and mechanism through the landslide distribution characteristics.

$$L = R^{*}\mathrm{Arccos}[\sin(Y1)^{*}\sin(Y2) + \cos(Y1)^{*}\cos(Y2)^{*}\cos(X1 - X2)]^{*}Pi/180 \quad (1)$$

where R is the radius of the Earth, and Pi is the circular constant.

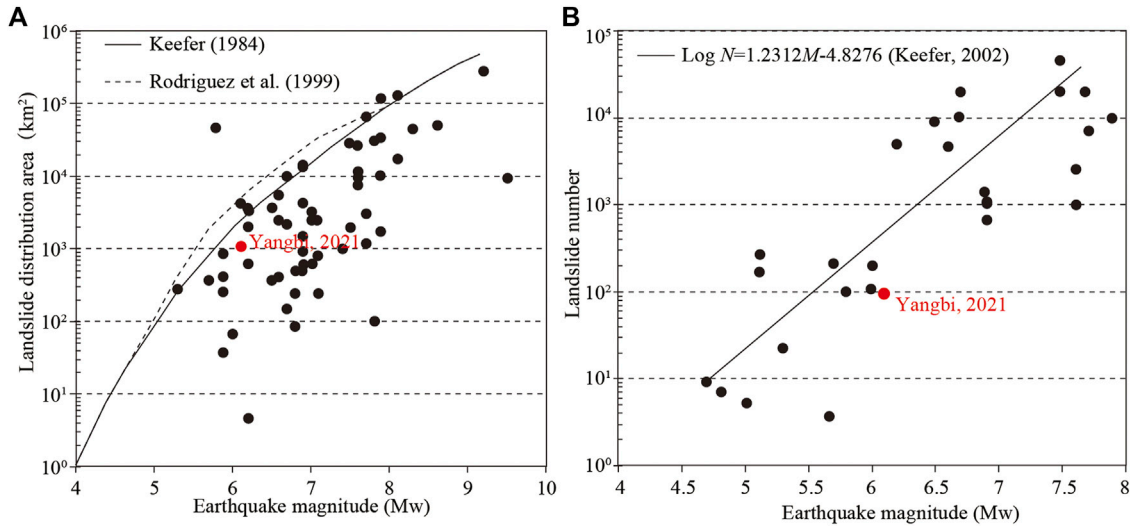

FIGURE 4
Correlations between earthquake magnitude (Mw) and co-seismic landslide distribution (affected) area **(A)** and the landslide number **(B)**. The cases shown by black circles references Keefer (1984, 2002), Rodriguez et al. (1999), Xu and Xu (2014) and He et al. (2021).

4 Distribution characteristics of co-seismic landslides

4.1 Landslide inventory

The results of the interpretation show that the landslides triggered by the Yangbi earthquake are mainly distributed in the VII-VIII seismic intensity zone, which is the area affected by the co-seismic landslides with an area of about 1,105 km^2 (Figure 2). The overall long axis of the distribution zone is in the NW-SE direction, which is consistent with the long axis of the seismic intensity contour (Figure 2). According to the relationship between the area affected by co-seismic landslide and earthquake magnitude suggested by Keefer (1984) and Rodriguez et al. (1999), most earthquake events are located below the given envelopes (the solid black line and dotted line in Figure 4). The Yangbi earthquake also conforms to this rule (Figure 4A). A total of 95 co-seismic landslides were identified in the region, with a total area of about 0.1 km^2. The area of these landslides ranges from 166.3 m^2 to 3489.6 m^2, and the average area of each landslide is about 999.5 m^2. Among them, 38 landslides are greater than 1000 m^2 in area. According to the relationship between landslide number and the earthquake magnitude proposed by Keefer (2002), the number of landslides induced by the Yangbi earthquake is relatively smaller than earthquakes of the same magnitude. It lies below the fitted line (Figure 4B). However, the logarithmic relationship between the area (A) and the number (N) of co-seismic landslides with an area less than A (Xu et al., 2014; Xu et al., 2015) can ideally be expressed as lgN = a × lgA + b (a and b are coefficients), which illustrates the completeness of the co-seismic landslide inventory. Figure 5 demonstrates the relationship between the cumulative number (N) of Yangbi earthquake-triggered landslides and the area (A) of a single landslide. The fit relationship of all values on the logarithmic axis is consistent with the ideal state, with coefficients a and b of −1.1946 and 5.0195, respectively. The fit line's coefficient of determination

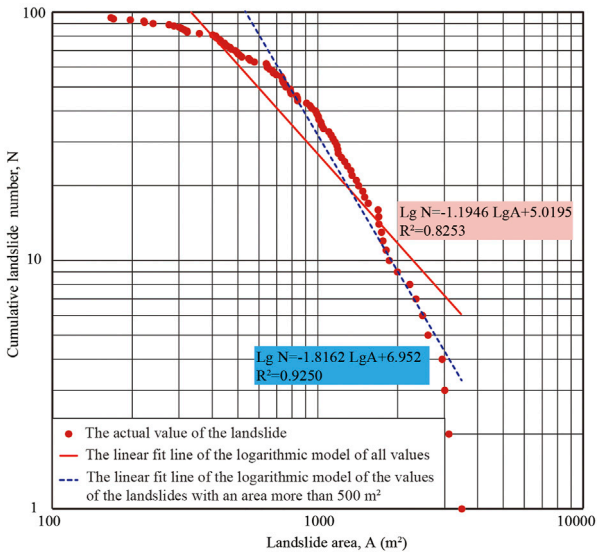

FIGURE 5
Correlation between the cumulative landslide number and the landslide area related to the Yangbi earthquake.

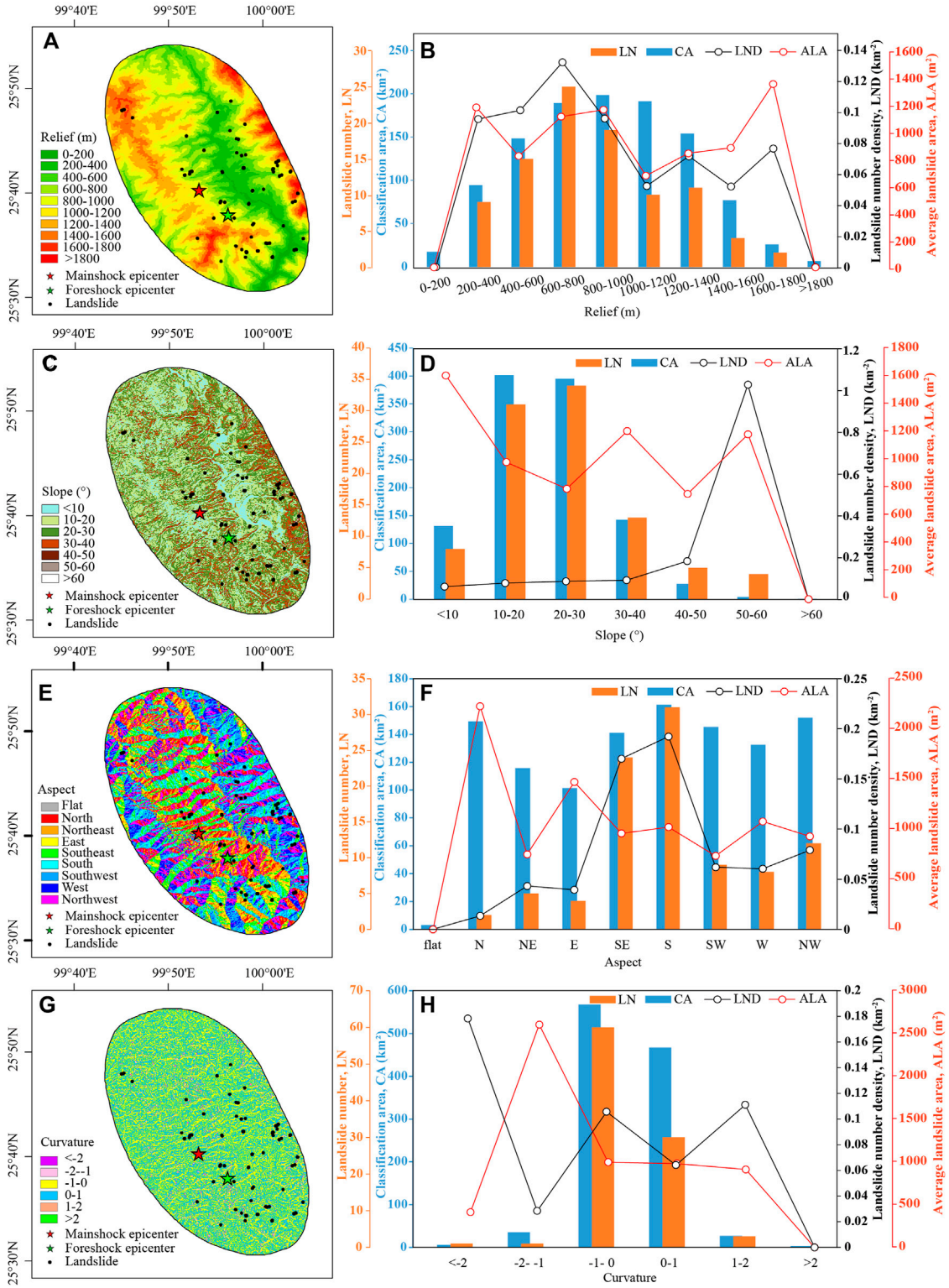

FIGURE 6
The landslide distribution in classifications of topographical factors (left) and their correlations (right). **(A,B)** Topographic relief. **(C,D)** Slope angle. **(E,F)** Slope aspect. **(G,H)** Slope curvature. LN: Landslide number; LND: landslide number density; CA: classification area; ALA: average landslide area.

(R^2) is as high as 0.83, indicating that the catalogs of Yangbi earthquake-triggered landslides are relatively complete. The R^2 of the landslides with area more than 500 m^2 is up to 0.93. The closer R^2 is to 1, the higher the fit is and the more complete the compiled landslides are. The results indicate that some small-scale landslides were not identified, probably due to the constraint of satellite image resolution.

4.2 Distribution of landslides in classifications of influence factors

4.2.1 Topographical factors

The maximum topographic relief in the study area is 2,355 m, but there are fewer areas with relief of more than 1800 m. The relief of most of the area is mainly 600–1,200 m (Figures 6A,B). There are the largest landslide number and number densities and relatively larger average landslide area in the area with the relief 600–800 m. The largest average landslide area is in the region with the relief of 1,600–1800 m (Figure 6B). No landslide occurred in the area with relief of 0–200 m and above 1800 m due to the small area. Overall, there is no apparent rule between relief and landslide distribution.

The slope angle range is 0–70.9° in the study area. The area with a slope angle of 10–30° is dominant, while the area with a slope angle more significant than 60° only accounts for 0.04% of the whole area, so the number of landslides in the area of 10–30° is the largest. In comparison, no landslides occur in the area above 60° (Figures 6C,D). As shown in Figure 6D, the landslide density in the study area increases with the slope angle except for the area above 60°. Still, the average landslide area in the area with a slope angle of less than 10° is the largest. It shows that the larger the slope angle is, the more likely the co-seismic landslide will occur. Although the low-angle slope is not prone to landslides, the scale of landslides will be more significant once it occurs.

The area of classifications of aspects in the study area is relatively average, and that of the flat surface is small, where there is no landslide (Figures 6E,F). The peaks of LN and LND occur on the south and southeast-facing slopes, while the peak of ALA is on the slopes facing north (Figures 6E,F). It indicates that the co-seismic landslides mainly occur on the slopes facing south and southeast, and there are fewer landslides on the north-facing slopes, but with a larger average landslide area.

Slope curvature may also affect landslide distribution. A negative curvature indicates a concave slope and a positive curvature indicates a convex slope. A slope with zero or near zero curvature is a flat slope. As shown in Figures 6G,H, most of the slopes in the study area are relatively flat (curvature of -1 to 1), and most landslides occur on this type of slope. Slope areas with greater concavity are small, where only a few landslides arise, but their landslide density or average size is occasionally larger. There is no significant positive or negative correlation between the distribution of landslides and the slope curvature.

4.2.2 Seismic factors

Figure 7 shows the relationship between the distribution of landslides and the distance from the epicenters of the Yangbi mainshock and foreshock. Most landslides occurred in the area with a distance of 10–20 km from the mainshock epicenter, but the average landslide area in this area was smaller than those in other areas (Figures 7A,B). No landslides occurred in the area with a distance less than 2 km from the mainshock, and the landslide number density is most significant in the area with a distance of 2–4 km (Figure 7B). If the foreshock epicenter is centered, the landslides are mainly concentrated in the range of 16 km, during which there are several peaks of LN and LND, and the average landslide area in the area within 6 km is larger (Figures 7C,D). Combining the mainshock and foreshock epicenters, we found that the LN and LND show multi-peak characteristics, occurring at the zones of 2–4 km, 6–8 km, and 12–14 km, respectively, but the size of landslides (ALA) generally show a trend of decreasing with the increase of the distance from epicenters (Figures 7E,F). The above analysis shows that the development of the co-seismic landslides in the Yangbi earthquake is not only related to the location of the mainshock epicenter, but also influenced by the location of the foreshock epicenter, and the foreshock especially is related to the size of the landslides.

The relationship between the Yangbi earthquake intensity and the scale or number of landslides is evident in from Figures 8A,B. The maximum seismic intensity is VIII degree, and the area of the VIII-degree zone is 170.17 km^2. The area of the VII-degree intensity zone is 935.25 km^2, accounting for 84.60% of the total area of the study area. Although the number of landslides in the VII-degree intensity zone is more significant than that in the VIII-degree intensity zone, the landslide density and scale are smaller (Figures 8A,B). It can be concluded that the distribution characteristics of Yangbi earthquake-induced landslides conform to the relationship between co-seismic landslides and seismic intensity: the greater the intensity is, the more prone landslides occur, and the larger the scale of landslides is.

We compare the coseismic deformation and the landslide distribution in Figures 8C,D. The InSAR coseismic displacement field is characterized by a double-lobe pattern with a peak of ~9 cm (Figure 8C, Liu et al., 2022). More landslides are located at the southeast deformation lobe and the peaks of the LN and LND appears in the area with the displacement of 1–2 cm (Figure 8D). Notably, the size of deformation affects the size of landslide. The larger the deformation is, the larger the average landslide area generally is (Figure 8D).

4.2.3 Geological factors

As shown in Figures 8E,F, the area of Jurassic strata is the largest in the study area, but the number of landslides is not the largest there. The Jurassic strata are mainly composed of

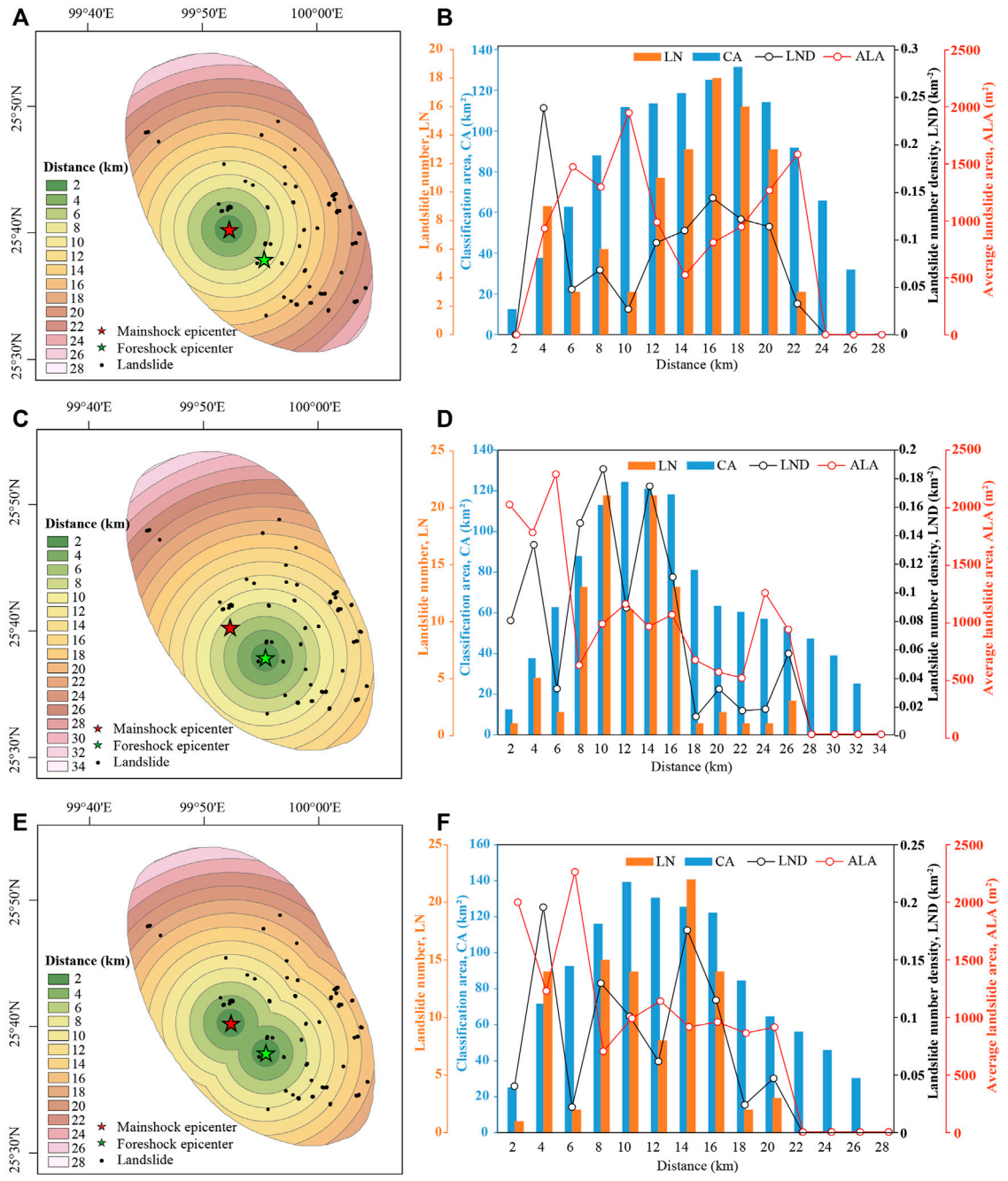

FIGURE 7
The correlations between landslide distribution and the distance to epicenters of mainshock and foreshock of the Yangbi earthquake. **(A,B)** The Ms 6.4 mainshock. **(C,D)** The Ms 5.6 foreshock. **(E,F)** The combination of the mainshock and foreshock. LN: Landslide number; LND: landslide number density; CA: classification area; ALA: average landslide area.

mudstone, sandstone and conglomerate, interspersed with marl and andesite. The LN and LND are the largest in the Triassic (Figures 8E,F), consisting mainly of mudstones, siltstones, tuffs, dolomites, and metamorphic rocks such as metamorphic mudstones, gneisses, and schists. Although the number of landslides in the Tertiary is small, its average landslide area is the most significant (Figures 8E,F). The Tertiary is also mainly mudstone, sandstone and conglomerate, but its consolidation degree is lower than that of Jurassic and Triassic. The lithology of the Cretaceous is especially metamorphic rocks, such as quartzite, slate, micrite, schist, dacite, *etc.* The LND of this formation is second only following the Triassic, but the ALA

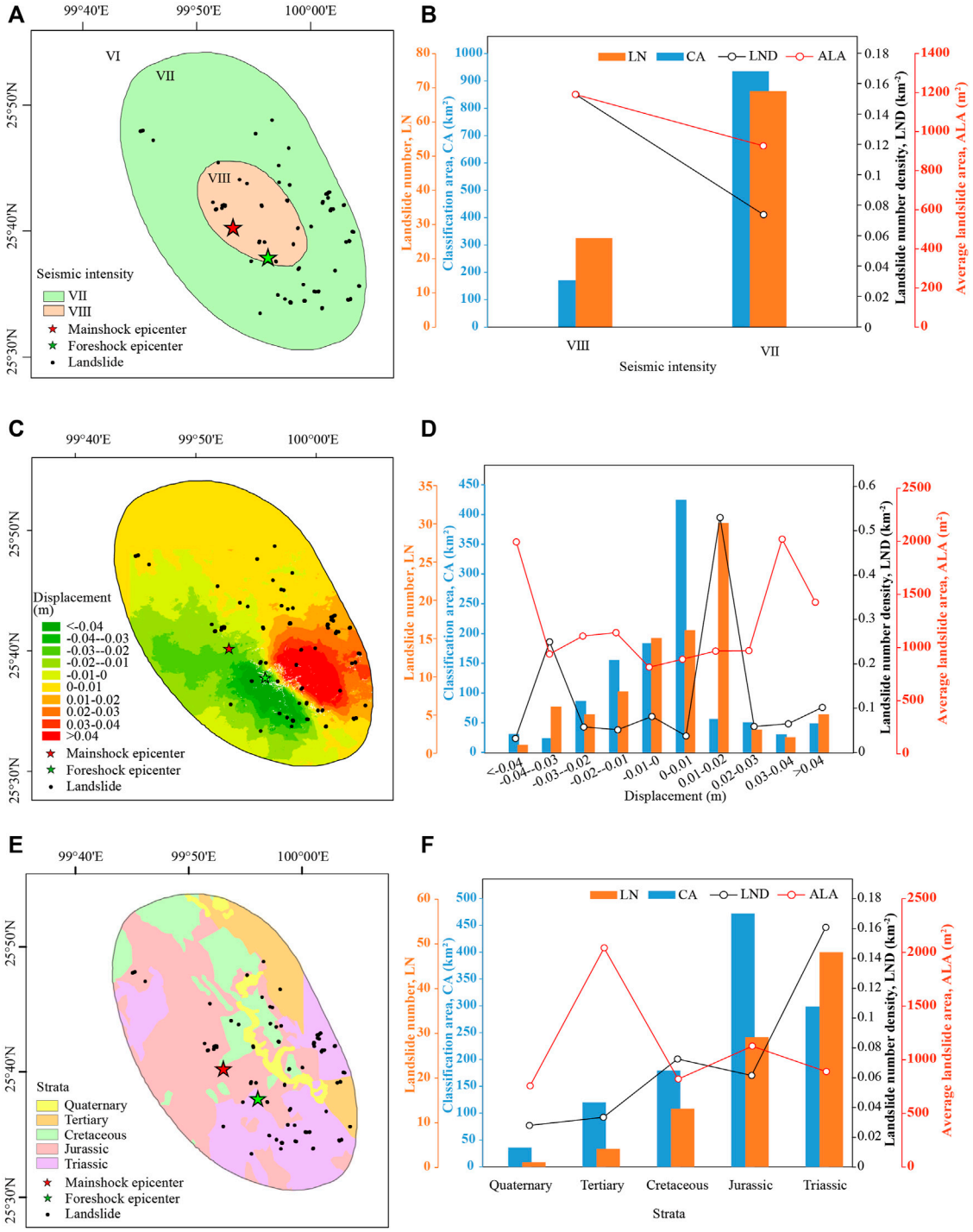

FIGURE 8
The correlations between landslide distribution and the seismic intensity **(A,B)**, co-seismic deformation **(C,D)**, and regional stratigraphy **(E,F)**. LN: Landslide number; LND: landslide number density; CA: classification area; ALA: average landslide area.

is relatively more minor (Figures 8E,F). There are fewer Quaternary strata in the study area, and the number and scale of landslides are small (Figures 8E,F).

Figures 9A,B show the distribution of landslides in the parallel zones of the WQWF. This fault zone consists of several parallel secondary faults, located within the strips of

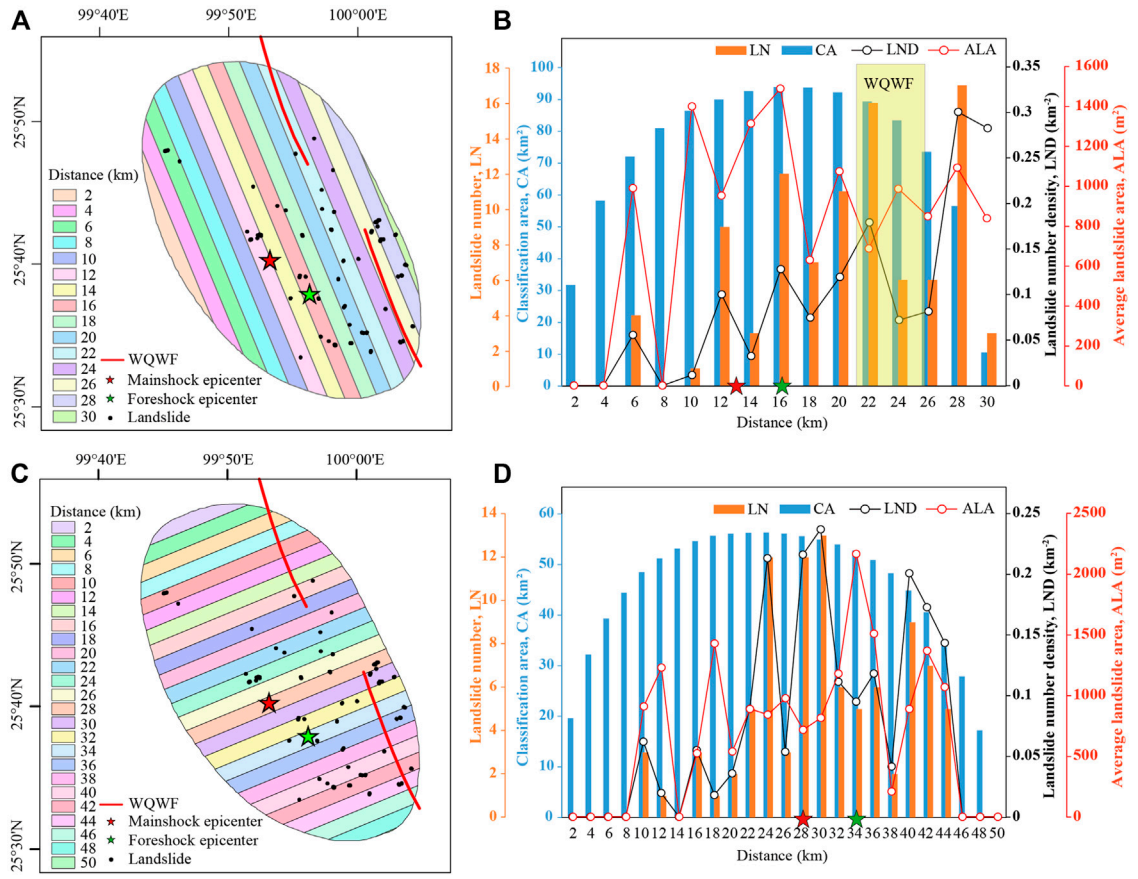

FIGURE 9
The correlations between landslide distribution and the Weixi-Qiaohou-Weishan fault (WQWF). **(A,B)** The vertical distance from the WQWF. **(C,D)** The parallel distance along the WQWF. LN: Landslide number; LND: landslide number density; CA: classification area; ALA: average landslide area.

22–26 km (Figures 9A,B). The landslides are mainly distributed in the southwest wall of the WQWF, and the relatively larger peaks of LN and LND occur in the southwest boundary zone and within 2 km to the northeast (i.e. the strip of 26–28 km) of the WQWF (Figure 9B). In the southwest wall, the LND generally decreases with increased vertical distance from the fault zone with multiple fluctuations (Figure 9B). However, the ALA is larger within the strips of 10–16 km, where the mainshock and foreshock epicenters are located (Figure 9B).

The distribution of landslides in the vertical zones of the WQWF is shown in Figures 9C,D. Most landslides occur in the zones close to the epicenters, and more landslides are located in the southeast section of the fault (Figures 9C,D). The zone with the peak average landslide area is the region where the epicenter of the foreshock is located, and the average area of landslides distributed at both ends along the fault is also relatively larger (Figures 9C,D). This may be due to the stress concentration effect of the earthquake at the ends of the rupture zone.

4.3 Mobility indices of the landslides

Landslide mobility index (H/L) is a parameter that characterizes the movement capacity of landslides. The smaller the H/L, the stronger the movement capacity of landslides and *vice versa*. Figure 10 shows the relationship between the slope angle, the area of the landslides, and the H/L ratio. The slope angle of the landslide is taken from the slope angle of the point representing the center of gravity. The results show that the H/L value of most landslides is less than 1. The change of H/L is no obvious pattern with the area of landslides (Figure 10), which indicates that the horizontal slip distance of most landslides is more significant than their elevation difference, and the motility of these landslides is not well correlated with the scale of the landslides. Additionally, the high linear relationship between the H/L value and the tangent of the slope angle indicates that the slope angle of the landslide mainly determines the H/L value; the H/L value increases with the increase of the slope angle (Figure 10). The slope of the fitted

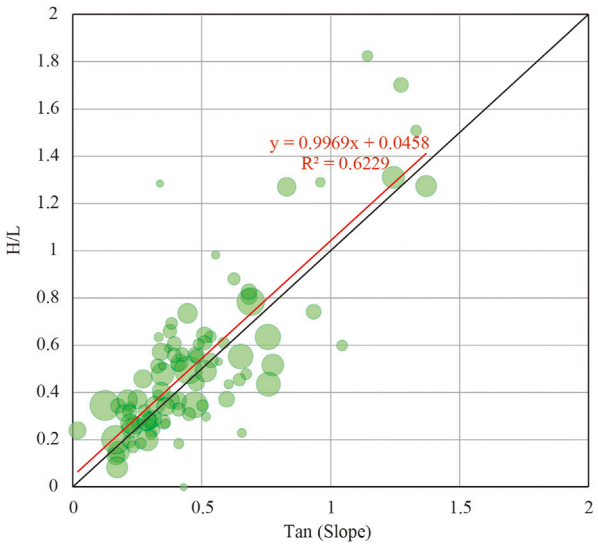

FIGURE 10
Relationship between the slope angle and H/L. The circle size indicates the size of the landslide. The solid red line is the linear fitting line.

line between the tangent of the slope angle and the H/L value is close to 1, which indicates that the motion pattern of the Yangbi earthquake-induced landslides fits well with the geometric triangle Pythagorean theorem of the slope.

5 Discussion

5.1 Effective controls on the Yangbi earthquake-triggered landslides distribution

Earthquake-induced landslides are mainly caused by seismic energy disturbing the ground surface. The responses of different topography, stratigraphy and faults to seismic energy vary, so the landslide distribution pattern is interactively controlled by seismic, topographic and geological factors, *etc.* (Gorum et al., 2011; Xu et al., 2014; Tanyaş et al., 2017; Roback et al., 2018; Tanyaş et al., 2019; Shao and Xu, 2022). According to the above results, slope angle and slope direction are the topographic factors that effectively influence the Yangbi earthquake-triggered landslides distribution (Figure 6). The slope angle is resonablely proportional to the susceptibility of co-seismic landslides in the Yangbi earthquake; the greater the slope angle, the more likely landslides will occur (Figures 6C,D). Additionally, the slope angle also affects the mobility of the landslide; the larger the slope angle, the larger the mobility of the landslide (Figure 10). It attributes to the steep slopes being less stable and prone to failure (Gorum et al., 2013; Xu et al., 2015), and the larger slope angle leads to a larger component of gravity on the slope, which results in a larger acceleration of the slider and an increase in slip distance. According to previous studies, the Yangbi earthquake rupture propagated mainly to the southeast direction with a southward deflection (Liu et al., 2021; Long et al., 2021), the co-seismic landslides occurred primarily in the slopes facing south and southeast (Figures 6E,F), showing a significant "back-slope effect". It means that in the gully slopes nearly perpendicular to the seismogenic rupture zone, the density of landslide on the backslope side of the seismic wave propagation is significantly greater than that on the facing slope side (Figure 11A; Xu and Li, 2010). In other words, the slopes with the aspect same as the propagation direction of the seismic wave are more likely to collapse than slopes facing the source (Shao et al., 2022). This phenomenon has also been observed in other earthquake cases, such as the 1999 Chi-Chi earthquake in Taiwan (Liao and Lee, 2000), the 2005 Kashmir earthquake (Sato et al., 2007), and the 2008 Wenchuan earthquake (Dai et al., 2011). Based on the stress wave theory, Tang et al. (2009) suggested that the "back-slope effect" might be related to the spalling phenomenon caused by the multiplication of reflected stretching waves when the compressional waves encounter the free surface of the slope. Xu and Li (2010) concluded that the refraction and reflection of propagation of seismic waves within slopes during earthquakes resulting the change in stress within the slopes might be used to explain "back-slope effect".

In terms of seismic factors, it is clear that the distribution of Yangbi earthquake-induced landslides is related to the seismic intensity; the greater the seismic intensity, the stronger the seismic damage energy, the larger the possibility of landslides, and the larger the scale of landslides (Figures 8A,B). This is the same as the previous understanding (Xu et al., 2015; He et al., 2021). It has been shown that the distance from the epicenter is negatively correlated with the number of landslides (Papadopoulos and Plessa 2000). However, the number or density of landslides does not decrease strictly with the increase of the distance from the mainshock's epicenter or the foreshock's, and there were multiple fluctuations in the process (Figure 7). Interestingly, the average landslide area generally increases with decreasing distance from the foreshock epicenter (Figure 7D), which is attributed to the region near the foreshock epicenter. The area was strongly affected by the foreshock, becoming more vulnerable and then being disturbed again by the mainshock to form larger-scale landslides. This shows that the foreshocks and the mainshock interact to control the distribution of the co-seismic landslides jointly.

In addition, the Yangbi earthquake-triggered landslides mainly occurred in metamorphic rocks (Figures 8E,F). Generally, the strength of metamorphic rocks has decreased after long-term geological action, and the weaker the rock strength is, the more favorable the landslides are in the area (Xu et al., 2015). Notably, the effect of the WQWF on landslide

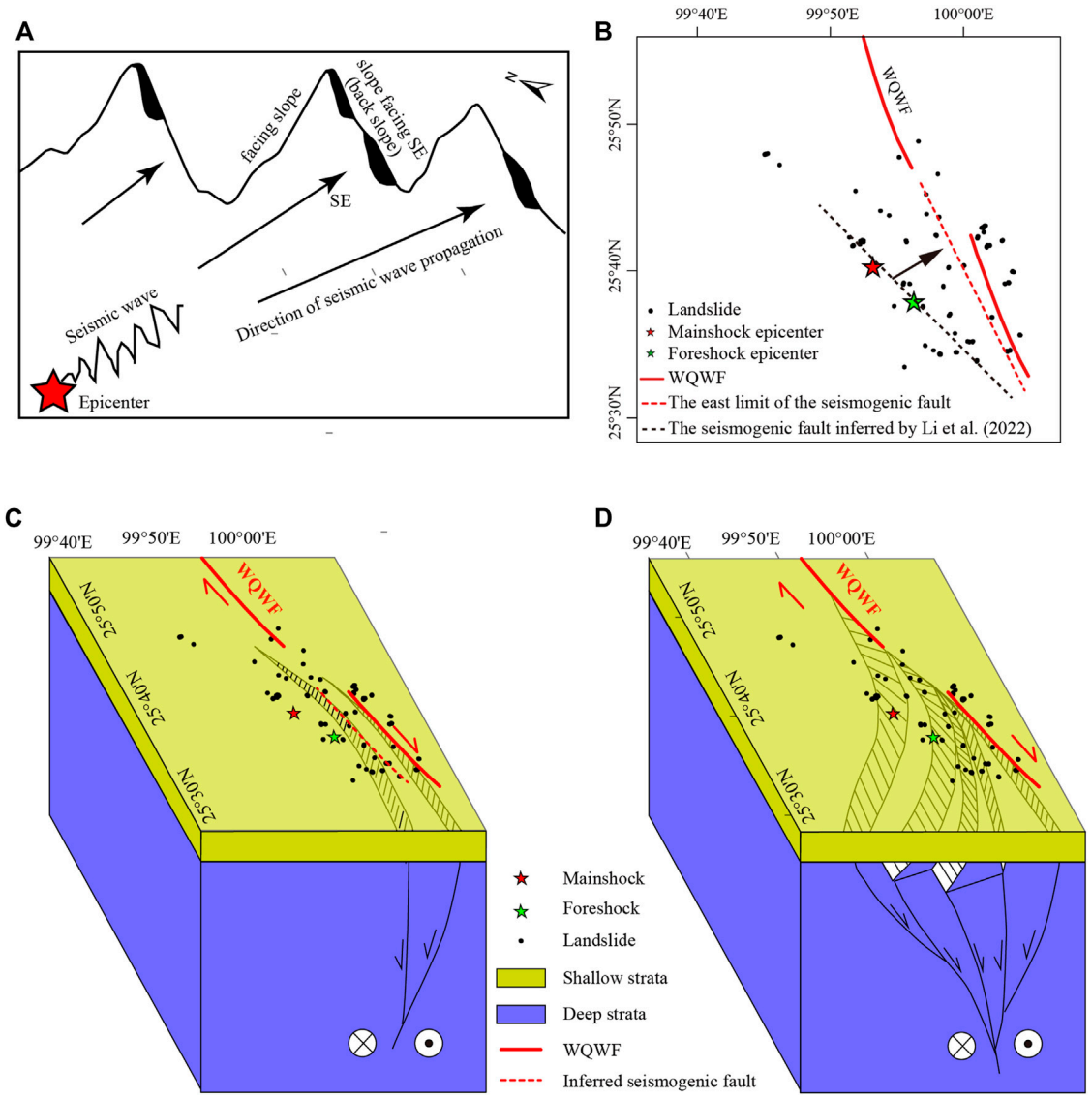

FIGURE 11
(A) Schematic diagram of "back-slope effect" of co-seismic landslide. **(B)** The map showing the inferred locations of the seismogenic structure. **(C)** Model of the seismogenic structure showing a parallel secondary fault of the WQWF. **(D)** Model of the associated flower structure in the southwest wall of the WQWF. Both models are mainly chararistized by right-lateral strike slip with a small amount of normal-fault component. WQWF: Weixi-Qiaohou-Weishan fault.

distribution is critical to analyze the seismogenic structure, which is explained in detail below.

5.2 Indication of landslide distribution patterns on the seismogenic structure

The earthquake-triggered landslides are generally controlled by the seismogenic structure and are linearly distributed along the seismogenic fault (Keefer 2000; Mahdavifar et al., 2006; Xu et al., 2014; Gorum et al., 2014; Valagussa et al., 2019). The distribution characteristics of co-seismic landslides vary with different fault types. For example, strike-slip earthquake-induced landslides are symmetrically distributed on both sides of the seismogenic fault (Gorum et al., 2014; He et al., 2021). Oblique-slip earthquake-induced landslides are mainly distributed in the hanging wall of the fault (Tatard and Grasso, 2013; Xu et al., 2014). Earthquakes occurring in blind faults generally do not cause surface rupture, and the landslides induced by them are small in scale and scattered (Xu, 2014). The study results show

that the long axis of Yangbi earthquake-induced landslide distribution area is about in the NW-SE direction, nearly parallel to the strike of the WQWF. The number and density of landslides in the neighboring strips on the west side of this fault zone are relatively larger and those are somewhat smaller except for the strip of 26–28 km on the east side of the WQWF (Figure 9B). Although there is a decreasing trend of the number and density of co-seismic landslides with increased vertical distance from the fault, there are more fluctuations (Figure 9B). Notably, the landslides are mainly distributed in the southwest wall of the fault. The landslides are asymmetric on both sides of the WQWF (Figure 9B). Combined with the feature that the landslides induced by a strike-slip earthquake is symmetrical on both sides of the seismogenic fault, the seismogenic structure is related to the WQWF, but is not the mapped main fault, and should be located in the west of the WQWF. The east limit of the seismogenic fault should be in the strip of 20–22 km according to the peaks of LND and LN (Figure 9B), shown with a red dotted line in Figure 11B. Li et al. (2022) used InSAR and GNSS observations to obtain co-seismic deformation and the inferred seismogenic fault, a secondary fault of the WQWF (the black dotted line in Figure 11B). The suspected seismogenic fault is about 10 km away from the WQWF. Through seismic sequence pinpointing, many studies showed that the Yangbi seismic sequence distributes along the NW-SE direction, which is approximately parallel to the WQWF with a distance of 3–10 km (Li et al., 2021; Long et al., 2021). Several studies show that the seismogenic fault dips to the southwest based on earthquake distribution (Long et al., 2021; Liu et al., 2022; Li et al., 2022; Zhang et al., 2022). According to the landslides are prone to occur on the hanging wall, the seismogenic fault should be moved eastward from the location inferred by Li et al. (2022) (Figure 11B). Therefore, we can infer one model that the Yangbi earthquake's seismogenic fault is a parallel associated fault of the WQWF, with the NW-SE striking, dipping toward the southwest with a large dip angle (Figure 11C). This model is supported by many studies based on the aftershock distribution (Yang et al., 2021; Li et al., 2021a, b). The relatively scattered distribution of landslides can be attributed to the absence of surface rupture. That is, the seismogenic fault is a blind fault (Yang et al., 2021), which is consistent with surface deformation deficit in 0–3 km depth (Li et al., 2022). However, Liu et al. (2021) suggested that the strike-slip fault accompanied a negative flower tectonic system in the aftershock area. Two of its internal fractures were seismogenic structures of the Yangbi earthquake. This model is shown in Figure 11D, which can be supported by multiple fluctuations of LND in the parallel strips of the WQWF (Figure 9B). The study results of the foreshock sequence show the foreshocks can be grouped into several episodes, which occurred in different small or secondary faults of the WQWF, and these faults even dip to different directions (Liu et al., 2022; Zhou et al., 2022; Zhu et al., 2022). Long et al. (2021) proposed the southeast section is more complex with a relatively slow dip angle and several branching structures based on the aftershock distribution. These characteristics are consistent with those of the WQWF. Therefore, the flower structural model in the southwest wall of the WQWF is a possible explanation for complex co-seismic landslide distribution, aftershocks distribution, and foreshock sequences. In summary, under the premise of obeying the characteristic of dominated right-lateral strike slip with a small amount of tension component, both of the above seismogenic structure models are, can reasonably explain the intricate landslide distribution pattern and the distribution of foreshocks and aftershocks to a certain extent. The formation of such a structure may be related to the SE-directional slip of the Sichuan-Yunnan block and the clockwise rotation of the southwest Yunnan block.

Additionally, along the fault, more landslides are distributed in the southeast section of the fault, referring to the main earthquake epicenter (Figure 9D). It is inferred that the earthquake rupture mainly propagates toward the southeast direction. This inference is confirmed by the distribution of aftershocks and co-seismic deformation. The mainshock is located in the northwest end of the dense aftershock area, indicating that it unidirectionally ruptured in the southeast direction (Liu et al., 2021; Long et al., 2021). Li et al. (2022) and Liu et al. (2022) showed the most significant co-seismic deformation is located in the southeast section, where more landslides caused by the 2021 Yangbi earthquake occurred (Figures 8C,D). This may indicate the co-seismic deformation toward the southeast relates to the landslides.

6 Conclusion

1) Based on the interpretation of remote sensing satellite images, we compiled the most detailed and complete inventory available, including 95 landslides induced by the 2021 Yangbi earthquake in Yunnan, China. The distribution of co-seismic landslides in the Yangbi earthquake is influenced by multiple factors. The slope angle is not only proportional to the probability of landslide occurrence, but also proportional to the landslide mobility. Landslides are more likely to appear on the south- and southeast-facing slopes, showing a significant "back-slope effect". Among the seismic factors, besides the seismic intensity, the distance from the epicenters of mainshock and foreshock also has an effect on the distribution of landslides. Significantly, the foreshock affects the size of the landslides. In addition, the landslides occurred mainly in the weaker metamorphic rocks and were closely related to the nearest WQWF system.

2) The long axis of the Yangbi earthquake-induced landslide distribution area is in the NW-SE direction, which is nearly parallel to the trending direction of the WQWF. The landslides are mainly distributed in the fault's southwest wall. The number and density

of landslides on west wall of the fault shows the overall trend of decline with the increase in vertical distance from the fault, but there are a lot of fluctuates. Combined with the previous studies, two models of the seismogenic structure of Yangbi earthquake can be inferred to explain the complex distribution pattern of the landslides. One is a parallel secondary fault of the WQWF, which is trending in the NW-SE direction Another one is the associated flower structure in the southwest wall of the WQWF. Both models are mainly right-lateral strike-slip with a small amount of normal-fault component. The landslides are mainly and relatively scattered in the southeast section of the seismogenic structure, which indicate the seismic rupture propagated mainly toward the southeast and was hidden under the surface without surface rupture.

Data availability statement

The raw data supporting the conclusions of this article will be made available by the authors, without undue reservation.

Author contributions

XH: Providing ideas, processing data, Drafting and writing the manuscript; CX: Providing ideas and methods and improving the manuscript.

Funding

This work was supported by the National Natural Science Foundation of China (42002225, 42077259).

Acknowledgments

We thank the reviewers as well as editors for providing constructive suggestions.

Conflict of interest

The authors declare that the research was conducted in the absence of any commercial or financial relationships that could be construed as a potential conflict of interest.

Publisher's note

References

Chang, Z. F., Chang, H., Zang, Y., and Dai, B. Y. (2016). Recent active features of Weixi-Qiaohou fault and its relationship with the Honghe fault. *J. Geomechanics* 22 (3), 517–530. doi:10.3969/j.issn.1006-6616.2016.03.009

Chang, Z. F., Zhang, Y., and Chang, H. (2018). New discovery of Holocene activity along the Weixi-Qiaohou fault in southeastern margin of the Tibetan Plateau and its Neotectonic significance. *Acta Geol. Sin. Engl. Ed.* 92 (6), 2464–2465. doi:10.1111/1755-6724.13751

Chang, Z. F., Zhang, Y. F., Li, J. L., and Zang, Y. (2014). The geological and geomorphic characteristic of late Quaternary activity of the Deqin-Zhongdian-Daju fault. *J. Seismol. Res.* 37 (1), 46–52. doi:10.3969/j.issn.1000-0666.2014.01.007

Chang, Z. L., Catani, F., Huang, F. M., Liu, G. Z., Meena, S. R., Huang, J. S., et al. (2022). Landslide susceptibility prediction using slope unit-based machine learning models considering the heterogeneity of conditioning factors. *J. Rock Mech. Geotechnical Eng.* doi:10.1016/j.jrmge.2022.07.009

Chang, Z. L., Du, Z., Zhang, F., Huang, F. M., Chen, J. W., Li, W. B., et al. (2020). Landslide susceptibility prediction based on remote sensing images and GIS: Comparisons of supervised and unsupervised machine learning models. *Remote Sens.* 12, 502. doi:10.3390/rs12030502

Dai, F. C., Tu, X. B., Xu, C., Gong, Q. M., and Yao, X. (2011). Rock avalanches triggered by oblique-thrusting during the 12 May 2008 Ms8.0 Wenchuan earthquake, China. *Geomorphology* 132 (3/4), 300–318. doi:10.1016/j.geomorph.2011.05.016

Deng, Q. D., Cheng, S. P., Ma, J., and Du, P. (2014). Seismic activities and earthquake potential in the Tibetan Plateau. *Chin. J. Geophys.* 57 (5), 678–697. doi:10.1002/cjg2.20133

Deng, Q. D., Zhang, P. Z., Ran, Y. K., Yang, X. P., Min, W., and Chu, Q. Z. (2003). Basic characteristics of active tectonics of China. *Sci. China Ser. D Earth Sci.* 46 (4), 356–372. doi:10.1360/03yd9032

Fan, X. M., Scaringi, G., Korup, O., West, A. J., van Westen, C. J., Tanyas, H., et al. (2019). Earthquake-induced chains of geologic hazards: Patterns, mechanisms, and impacts. *Rev. Geophys.* 57 (2), 421–503. doi:10.1029/2018rg000626

Gan, W. J., Molnar, P., Zhang, P. Z., Xiao, G. R., Liang, S. M., Zhang, K. L., et al. (2022). Initiation of clockwise rotation and eastward transport of southeastern Tibet inferred from deflected fault traces and GPS observations. *Bulletin* 134 (5-6), 1129–1142. doi:10.1130/B36069.1

Gorum, T., Fan, X. M., van Westen, C. J., Huang, R. Q., Xu, Q., Tang, C., et al. (2011). Distribution pattern of earthquake-induced landslides triggered by the 12 May 2008 Wenchuan earthquake. *Geomorphology* 133 (3–4), 152–167. doi:10.1016/j.geomorph.2010.12.030

Gorum, T., Korup, O., van Westen, C. J., van der Meijde, M., Xu, C., and van der Meer, F. D. (2014). Why so few? Landslides triggered by the 2002 denali earthquake, Alaska. *Quat. Sci. Rev.* 95, 80–94. doi:10.1016/j.quascirev.2014.04.032

Gorum, T., van Westen, C. J., Korup, O., van der Meijde, M., Fan, X. M., and van der Meer, F. D. (2013). Complex rupture mechanism and topography control symmetry of masswasting pattern, 2010 Haiti earthquake. *Geomorphology* 184, 127–138. doi:10.1016/j.geomorph.2012.11.027

Harp, E. L., and Jibson, R. W. (1995). *Inventory of landslides triggered by the 1994 Northridge, California earthquake*. United States: USGS.

Harp, E. L., Keefer, D. K., Sato, H. P., and Yagi, H. (2011). Landslide inventories: The essential part of seismic landslide hazard analyses. *Eng. Geol.* 122 (1/2), 9–21. doi:10.1016/j.enggeo.2010.06.013

He, X. L., Xu, C., Qi, W. W., Huang, Y. D., Cheng, J., Xu, X. W., et al. (2021). Landslides triggered by the 2020 qiaojia mw 5.1 earthquake, yunnan, China: Distribution, influence factors and tectonic significance. *J. Earth Sci.* 32 (5), 1056–1068. doi:10.1007/s12583-021-1492-1

Huang, F. M., Cao, Z. S., Guo, J. F., Jiang, S. H., and Guo, Z. Z. (2020a). Comparisons of heuristic, general statistical and machine learning models for landslide susceptibility prediction and mapping. *Catena* 191, 104580. doi:10.1016/j.catena.2020.104580

Huang, F. M., Cao, Z. S., Jiang, S. H., Zhou, C. B., and Guo, Z. Z. (2020c). Landslide susceptibility prediction based on a semi-supervised multiple-layer perceptron model. *Landslides* 17, 2919–2930. doi:10.1007/s10346-020-01473-9

Huang, F. M., Chen, J. W., Liu, W. P., Huang, J. S., Hong, H. Y., and Chen, W. (2022). Regional rainfall-induced landslide hazard warning based on landslide susceptibility mapping and a critical rainfall threshold. *Geomorphology* 408, 108236. doi:10.1016/j.geomorph.2022.108236

Huang, F. M., Zhang, J., Zhou, C. B., Wang, Y. H., Huang, J. S., and Zhu, L. (2020b). A deep learning algorithm using a fully connected sparse autoencoder neural network for landslide susceptibility prediction. *Landslides* 17 (1), 217–229. doi:10.1007/s10346-019-01274-9

Jiang, J. Z., Li, J., and Fu, H. (2019). Seismicity analysis of the 2016 Ms5. 0 Yunlong earthquake, Yunnan, China and its tectonic implications. *Pure Appl. Geophys.* 176 (3), 1225–1241. doi:10.1007/s00024-018-2067-7

Jiang, S. H., Huang, J., Huang, F. M., Yang, J. H., Yao, C., and Zhou, C. B. (2018). Modelling of spatial variability of soil undrained shear strength by conditional random fields for slope reliability analysis. *Appl. Math. Model.* 63, 374–389. doi:10.1016/j.apm.2018.06.030

Keefer, D. K. (2002). Investigating landslides caused by earthquakes––a historical review. *Surv. Geophys.* 23 (6), 473–510. doi:10.1023/A:1021274710840

Keefer, D. K. (1984). Landslides caused by earthquakes. *Geol. Soc. Am. Bull.* 95, 406–421. doi:10.1130/0016-7606(1984)95<406:lcbe>2.0.co;2

Keefer, D. K. (2000). Statistical analysis of an earthquake-induced landslide distribution the 1989 Loma Prieta, California event. *Eng. Geol.* 58, 231–249. doi:10.1016/S0013-7952(00)00037-5

Khattak, G. A., Owen, L. A., Kamp, U., and Harp, E. L. (2010). Evolution of earthquake-triggered landslides in the Kashmir himalaya, northern Pakistan. *Geomorphology* 115 (1/2), 102–108. doi:10.1016/j.geomorph.2009.09.035

Lei, X. L., Wang, Z. W., Ma, S. L., and He, C. R. (2021). A preliminary study on the characteristics and mechanism of the May 2021 Ms6.4 Yangbi earthquake sequence, Yunnan, China. *Acta Seismol. Sin.* 43 (3), 261–286. doi:10.11939/jass.20210100

Leloup, P. H., Lacassin, R., Tapponnier, P., Schärer, U., Zhong, D. L., Liu, X. H., et al. (1995). The Ailao Shan-Red river shear zone (Yunnan, China), tertiary transform boundary of Indochina. *Tectonophysics* 251 (1–4), 3–84. doi:10.1016/0040-1951(95)00070-4

Li, C. L., Shan, X. J., Zhang, G. H., Zhao, C. P., Gong, W. Y., and Zhang, Y. F. (2022). Slip kinematics of the 2021 Yangbi earthquake: Fore-main-aftershock sequence rupture along an unknown secondary fault of the Weixi–Qiaohou Fault. *Seismol. Soc. Am.* 93 (3), 1400–1412. doi:10.1785/0220210220

Li, C. Y., Zhang, J. Y., Wang, W., Sun, K., and Shan, X. J. (2021b). The seismogenic fault of the 2021 Yunnan Yangbi Ms6.4 earthquake. *Seismol. Geol.* 43 (3), 706–721. doi:10.3969/j.issn.0253-4967.2021.03.015

Li, D. H., Ding, Z. F., Wu, P. P., Liu, S., Deng, F., Zhang, X., et al. (2021a). The characteristics of crustal structure and seismogenic background of Yangbi Ms6.4 earthquake on May 21, 2021 in Yunnan Province, China. *Chin. J. Geophys.* 64 (9), 3083–3100. doi:10.6038/cjg2021P0405

Liao, H. W., and Lee, C. T. (2000). Landslides triggered by the Chi-Chi earthquake. in Proceedings of the 21st Asian Conference on Remote Sensing, Taipei, China, December 4–8, 2000 1, 383–388.

Liu, J. Q., Gan, W. J., Wang, G. M., Wang, Z. L., Zhang, Y., Cai, H. L., et al. (2021). Seismic moment tensor and seismogenic structure of the Yangbi Ms6.4 earthquake sequence on May 21, 2021 in Yunnan. *Chin. J. Geophys.* 64 (12), 4475–4487. doi:10.6038/cjg2021P0559

Liu, M., Li, H. Y., Li, L., Zhang, M., and Wang, W. T. (2022b). Multistage nucleation of the 2021 Yangbi ms 6.4 earthquake, yunnan, China and its foreshocks. *JGR. Solid Earth* 127, e2022JB024091. doi:10.1029/2022JB024091

Liu, X. G., Xu, W. B., He, Z. L., Fang, L. H., and Chen, Z. D. (2022a). Aseismic slip and cascade triggering process of foreshocks leading to the 2021 M w 6.1 Yangbi earthquake. *Seismol. Soc. Am.* 93 (3), 1413–1428. doi:10.1785/0220210263

Long, F., Qi, Y. P., Yi, G. X., Wu, W. W., Wang, G. M., Zhao, X. Y., et al. (2021). Relocation of the Ms6.4 Yangbi earthquake sequence on may 21, 2021 in yunnan Province and its seismogenic structure analysis. *Chin. J. Geophys.* 64 (8), 2631–2646. doi:10.6038/cjg2021O0526

Mahdavifar, M. R., Solaymani, S., and Jafari, M. K. (2006). Landslides triggered by the avaj, Iran earthquake of june 22, 2002. *Eng. Geol.* 86, 166–182. doi:10.1016/j.enggeo.2006.02.016

Meunier, P., Uchida, T., and Hovius, N. (2013). Landslide patterns reveal the sources of large earthquakes. *Earth Planet. Sci. Lett.* 363, 27–33. doi:10.1016/j.epsl.2012.12.018

Pan, R., Jiang, J. Z., Fu, H., and Li, J. (2019). Focal mechanism and focal depth determination of yunnan Yangbi Ms5.1 and Ms4.8 earthquakes in 2017. *J. Seismol. Res.* 42 (3), 338–348. doi:10.3969/j.issn.1000-0666.2019.03.005

Papadopoulos, G. A., and Plessa, A. (2000). Magnitude–distance relations for earthquake-induced landslides in Greece. *Eng. Geol.* 58, 377–386. doi:10.1016/S0013-7952(00)00043-0

Ren, J. J., Zhang, S. M., Hou, Z. H., and Liu, X. D. (2007). Study of late Quaternary slip rate in the mid-segment of the Tongdian-Weishan fault. *Seismol. Geol.* 29 (4), 756–764. doi:10.3969/j.issn.0253-4967.2007.04.006

Roback, K., Clark, M. K., West, A. J., Zekkos, D., Li, G., Gallen, S. F., et al. (2018). The size, distribution, and mobility of landslides caused by the 2015 Mw7. 8 Gorkha earthquake, Nepal. *Geomorphology* 301, 121–138. doi:10.1016/j.geomorph.2017.01.030

Rodriguez, C. E., Bommer, J. J., and Chandler, R. J. (1999). Earthquake-induced landslides: 1980–1997. *Soil Dyn. Earthq. Eng.* 18, 325–346. doi:10.1016/S0267-7261(99)00012-3

Sato, H. P., Hasegawa, H., Fujiwara, S., Tobita, M., Koarai, M., Une, H., et al. (2007). Interpretation of landslide distribution triggered by the 2005 Northern Pakistan earthquake using SPOT 5 imagery. *Landslides* 4 (2), 113–122. doi:10.1007/s10346-006-0069-5

Shao, X. Y., Ma, S. Y., and Xu, C. (2022). Distribution and characteristics of shallow landslides triggered by the 2018 Mw 7.5 Palu earthquake, Indonesia. *Landslides*. doi:10.1007/s10346-022-01972-x

Shao, X. Y., and Xu, C. (2022). Earthquake-induced landslides susceptibility assessment: A review of the state-of-the-art. *Nat. Hazards Res.* doi:10.1016/j.nhres.2022.03.002

Shen, Z. K., Lü, J. N., Wang, M., and Bürgmann, R. (2005). Contemporary crustal deformation around the southeast borderland of the Tibetan Plateau. *J. Geophys. Res.* 110, B11409. doi:10.1029/2004JB003421

Su, J. B., Liu, M., Zhang, Y. P., Wang, W. T., Li, H. Y., Yang, J., et al. (2021). High resolution earthquake catalog building for the 21 May 2021 Yangbi, Yunnan, Ms6.4 earthquake sequence using deep-learning phase picker. *Chin. J. Geophys.* 64 (8), 2647–2656. doi:10.6038/cjg2021O0530

Tang, C. A., Zuo, Y. J., Qin, S. F., Yang, J. Y., Wang, D. G., Li, L. C., et al. (2009). "Spalling and slinging i pattern of shallow slope and dynamics explmration in the 2008 Wenehuan earthquake," in Proceedings of the 10th Conference on Rock Mechanics and Engineering, Chengdu, China, April 25, 2009, 258–262. China.

Tanyaş, H., Van Westen, C. J., Allstadt, K. E., Anna Nowicki Jessee, M., Görüm, T., Jibson, R. W., et al. (2017). Presentation and analysis of a worldwide database of earthquake-induced landslide inventories. *J. Geophys. Res. Earth Surf.* 122 (10), 1991–2015. doi:10.1002/2017JF004236

Tanyaş, H., van Westen, C. J., Allstadt, K. E., and Jibson, R. W. (2019). Factors controlling landslide frequency–area distributions. *Earth Surf. Process. Landf.* 44 (4), 900–917. doi:10.1002/esp.4543

Tapponnier, P., Lacassin, R., Leloup, P. H., Schärer, U., Zhong, D. L., Wu, H. W., et al. (1990). The ailao Shan/Red River metamorphic belt: Tertiary left-lateral shear between indochina and south China. *Nature* 343 (6257), 431–437. doi:10.1038/343431a0

Tapponnier, P., Zhiqin, X., Roger, F., Meyer, B., Arnaud, N., Wittlinger, G., et al. (2001). Oblique stepwise rise and growth of the Tibet Plateau. *Science* 294 (5547), 1671–1677. doi:10.1126/science.105978

Tatard, L., and Grasso, J. R. (2013). Controls of earthquake faulting style on near field landslide triggering: The role of coseismic slip. *J. Geophys. Res. Solid Earth* 118 (6), 2953–2964. doi:10.1002/jgrb.50215

Valagussa, A., Marc, O., Frattini, P., and Crosta, G. B. (2019). Seismic and geological controls on earthquake-induced landslide size. *Earth Planet. Sci. Lett.* 506, 268–281. doi:10.1016/j.epsl.2018.11.005

Wang, G. M., Peng, G. L., Zhao, X. Y., and Fu, H. (2021). Seismic risk of the Weixi-Qiaohou fault zone based on temporal-spatial distribution characteristics of earthquake sequences. *J. or Seismol. Res.* 44 (3), 367–379. doi:10.3969/j.issn.1000-0666.2021.03.008

Wang, Q., Zhang, P. Z., Freymueller, J. T., Bilham, R., Larson, K. M., Lai, X. A., et al. (2001). Present-day crustal deformation in China constrained by global positioning system measurements. *Science* 294 (5542), 574–577. doi:10.1126/science.1063647

Xu, C. (2014). Do buried-rupture earthquakes trigger less landslides than surface-rupture earthquakes for reverse faults? *Geomorphology* 216, 53–57. doi:10.1016/j.geomorph.2014.03.029

Xu, C. (2015). Preparation of earthquake-triggered landslide inventory maps using remote sensing and GIS technologies: Principles and case studies. *Geosci. Front.* 6 (6), 825–836. doi:10.1016/j.gsf.2014.03.004

Xu, C., Xu, X. W., and Shyu, J. B. H. (2015). Database and spatial distribution of landslides triggered by the Lushan, China Mw 6.6 earthquake of 20 April 2013. *Geomorphology* 248, 77–92. doi:10.1016/j.geomorph.2015.07.002

Xu, C., and Xu, X. W. (2014). Statistical analysis of landslides caused by the Mw 6.9 Yushu, China, earthquake of April 14, 2010. *Nat. Hazards (Dordr).* 72 (2), 871–893. doi:10.1007/s11069-014-1038-2

Xu, C., Xu, X. W., Yao, X., and Dai, F. C. (2014a). Three (nearly) complete inventories of landslides triggered by the May 12, 2008 Wenchuan Mw 7.9 earthquake of China and their spatial distribution statistical analysis. *Landslides* 11 (3), 441–461. doi:10.1007/s10346-013-0404-6

Xu, Q., and Li, W. (2010). Study on the direction effects of landslides triggered by wenchuan earthquake. *J. Sichuan Univ. Eng. Sci. Ed.* 42 (1), 7–14.

Xu, T., Zhang, M. H., Tian, X. B., Zheng, Y., Bai, Z. M., Wu, C. L., et al. (2014b). Upper crustal velocity of Lijiang-Qingzhen profile and its relationship with the seismogenic environment of the Ms6.5 Ludian earthquake. *Chin. J. Geophys.* 57 (9), 3069–3079. doi:10.6038/cjg20140932

Xu, X. W., and Xu, C. (2021). Natural hazards research: An eternal subject of human survival and development. *Nat. Hazards Res.* 1 (1), 1–3. doi:10.1016/j.nhres.2020.12.003

Yang, J. Y., Wen, Y. M., and Xu, C. J. (2021a). The 21 may 2021 Ms 6.4 Yangbi (yunnan) earthquake: A shallow strike-slip event rupturing in a blind fault. *Chin. J. Geophys.* 64 (9), 3101–3110. doi:10.6038/cjg2021P0408

Yang, Z. G., Liu, J., Zhang, X. M., Deng, W. Z., Du, G. B., and Wu, X. Y. (2021b). A preliminary report of the Yangbi, Yunnan, M S 6.4 earthquake of May 21, 2021. *Earth Planet. Phys.* 5 (4), 1–3. doi:10.26464/epp2021036

Ye, T., Chen, X. B., Huang, Q. H., and Cui, T. F. (2021). Three-dimensional electrical resistivity structure in focal area of the 2021 Yangbi MS6.4 Earthquake and its implication for the seismogenic mechanism. *Chin. J. Geophys.* 64 (7), 2267–2277. doi:10.6038/cjg2021O0523

Yunnan Earthquake Bureau. (2021). The earthquake intensity map of the Ms6.4 Yangbi, Yunnan. Available at: http://www.yndzj.gov.cn/yndzj/_300559/_300651/629959/index.html.

Zhang, P. Z., Shen, Z. K., Wang, M., Gan, W. J., Bürgmann, R., Molnar, P., et al. (2004). Continuous deformation of the Tibetan Plateau from global positioning system data. *Geol.* 32 (9), 809–812. doi:10.1130/G20554.1

Zhang, Y. Y., An, Y. R., Long, F., Zhu, G. H., Qin, M., Zhong, Y. S., et al. (2022). Short-term foreshock and aftershock patterns of the 2021 M s 6.4 Yangbi earthquake Sequence. *Seismol. Soc. Am.* 93 (1), 21–32. doi:10.1785/0220210154

Zhao, X. Y., and Fu, H. (2014). Seismogenic structure identification of the 2013 Eryuan Ms5.5 and Ms5.0 earthquake sequence. *Acta Seismol. Sin.* 4, 640–650. doi:10.3969/j.issn.0253-3782.2014.04.010

Zhou, H. X., Che, A., and Li, G. (2022a). Characteristics and failure mechanism of landslides along highways triggered by 2021 Ms6.4 Yangbi earthquake. *Landslides* 19 (1), 165–176. doi:10.1007/s10346-021-01814-2

Zhou, Y. J., Ren, C. M., Ghosh, A., Meng, H. R., Fang, L. H., Yue, H., et al. (2022b). Seismological characterization of the 2021 Yangbi foreshock-mainshock sequence, yunnan, China: More than a triggered cascade. *JGR. Solid Earth* 127, e2022JB024534. doi:10.1029/2022JB024534

Zhu, G. H., Yang, H. F., Tan, Y. J., Jin, M. P., Li, X. B., and Yang, W. (2022). The cascading foreshock sequence of the ms 6.4 Yangbi earthquake in yunnan, China. *Earth Planet. Sci. Lett.* 591, 117594. doi:10.1016/j.epsl.2022.117594